POLYTECHNIC UNIVERSITY OF BUCHAREST

ELECTRICAL ENGINEERING DOCTORAL SCHOOL

DOCTORAL THESIS
Doctoral Thesis Summary

Studies concerning an HTS superconducting electromagnet for intense and uniform magnetic field

Scientific Adviser

Prof. PhD. Eng. Alexandru – Mihail Morega

Doctoral Student

Eng. Dan Enache

BUCHAREST 2021

This page is intentionally left blank

Summary

Keywords: superconduction, superconducting materials, LTS, HTS, magnetic field, heat transfer, physical model, mathematical model, numerical modeling, dipole superconducting electromagnet, superconducting coils, cryogenic cooling system, cryocooler, EMSD, electrodynamic forces, deformations, cryostat, HTS current conductors, superconducting junctions, experimental model.

DOCTORAL THESIS CHAPTERS STRUCTURE

The doctoral thesis “Studies concerning an HTS superconducting electromagnet for intense and uniform magnetic field” is structured in 7 chapters, conclusions and bibliography.

Chapter 1, “Superconductibility (theoretical aspects)”, presents introduction aspects regarding the theory of superconducting phenomenon. Subchapter 1.1, “Electrical conduction in classical theory”, contains a summary of classical electrical conduction theory. In subchapter 1.2, “Electrical conduction in the theory of superconducting materials”, the transition is made from the classical theory to that of superconducting materials and two important theories are presented, 1.2.1. “London Theory” and 1.2.2. "Ginzburg-Landau Theory".

In Chapter 2, “Superconducting Materials. Properties”, the types of superconducting materials, their properties and applications are treated. Subchapter 2.1, "Type I and II superconducting materials" presents the two types of superconducting materials. In subchapters 2.2, “LTS superconducting materials” and 2.3, “HTS superconducting materials”, the superconducting materials divided into two categories depending on the operating temperature, are presented. Further, in subchapter 2.4, “HTS materials with practical applicability” are presemted, emphasizing 2.4.1, “Requirements for practical use”, 2.4.2, “Commercially available HTS materials” and 2.4.3, “Properties and characteristics of HTS materials”. In 2.5, “Applications of HTS superconducting materials” a series of applications for HTS materials are presented.

Chapter 3, “The physical model” represents the step preceding the numerical modeling in which 3.1, “Physical model – the electromagnetic field problem” is described, namely in more detail 3.1.1, “The stationary electromagnetic field model in superconducting electromagnet”, respectively subchapter 3.2, “Heat transfer problem”.

Chapter 4, “Designing the EMSD Experimental Model” contains 4.1, “ HTS electromagnet overview”, 4.2, “EMS Conceptual Model” focusing on 4.2.1, “General characteristics” and 4.2.2, “Description of the EMSD Conceptual Model”, 4.3,“Superconducting coils”, 4.4,“Cryogenic cooling system”, 4.5,“Characteristics of HTS current conductors”.

Chapter 5, “Designing using numerical modeling of dipole superconducting electromagnet”, contains 5.1, “Current status”, a brief description of EMSD in 5.2, “Superconducting dipole electromagnet”, 5.3, “Design and numerical modeling of EMSD - magnetic field” where 5.3.1, “Uniform field excitation winding”, 5.3.2, “Analytical model for the calculation of the magnetic field” and 5.3.2, “ Numerical model for magnetic field evaluation” are presented. Electrodynamic forces are described in 5.4, "Design using numerical modeling of EMSD - electrodynamic forces - 2D". In 5.5, “Evaluation of the electrodynamic forces produced by the magnetic field of

EMSD - 3D", Laplace forces are studied in 3D, namely 3.5.1, "Identification of the areas most required by electrodynamic forces", respectively 3.5.2, "Evaluation of deformations that may occur in EMSD, following the actions of electrodynamic forces". Heat transfer is studied in subchapter 5.6, "Design and numerical modeling of EMSD - heat transfer", where in addition to the numerical evaluation of thermal loads in the system, an analytical model for calculating these thermal loads is presented in 5.6.1, "Analytical calculation of the thermal loads produced by the system (supported by the cryocooler)". A subchapter is dedicated to the study of superconducting junctions, 5.7, "Numerical modeling of the superconducting junctions operation".

In Chapter 6, "Development of experimental model for EMSD", 6.1, "Development of the experimental model" and 6.2, "Assembling the EMSD experimental model" are presented.

Chapter 7, "Testing the superconducting electromagnet", presents the experimental and measurement part of the thesis. The tests performed and presented in subchapter 7.1, "Tests and experiments performed on EMSD" are 7.1.1, "Testing vacuum conditions in cryostat", 7.1.2, "Testing the functional parameters of the cryocooler", 7.1.3, "Measurement of the characteristic parameters of the superconducting coils"and 7.1.4,"Magnetic field measurement generated by EMSD". In 7.2, "Junctions experimental measurement", the results obtained from the testing of superconducting junctions are presented.

Chapter 8 highlights the general conclusions of the scientific research and the results obtained in this thesis in the field of superconducting electromagnets, personal contributions to this paper and prospects for further development.

CHAPTER 1. SUPERCONDUCTIBILITY (THEORETICAL ASPECTS)

This chapter presents introduction aspects on the theory of the superconducting phenomenon.

1.1. Electrical conduction in classical theory

An electric field **E** induces an electric current in a metal. The connection between the electric field **E** and current density **J** it is given by Ohm's law

$$\mathbf{J} = \sigma \mathbf{E}, \tag{1.1}$$

where σ is the electrical conductivity of the material.

These are described by the empirical expression for net resistivity, also called the Matthiessen rule

$$\rho = \rho_L + \rho_i, \tag{1.2}$$

where $\rho_L[\Omega m]$ is the resistivity resulted from the electron-phonon interaction, and $\rho_i[\Omega m]$ represents the resistivity due to network imperfections. In general, the resistivity of a conductor decreases with decreasing temperature.

Inside a superconductor the magnetic flux density is $\mathbf{B} = 0$.

$$\frac{\partial \mathbf{B}(x)}{\partial t} = \frac{\partial \mathbf{B}(0)}{\partial t} e^{-x/\lambda}, \tag{1.3}$$

where *x* represents the distance from the conductor surface. Following this result it is assumed that **B** is constant in ratio to time inside of a perfect conductor, not necessarily zero. If the perfect conductor was placed in a magnetic field, and then entered in the perfect conduction state, that magnetic flux is kept inside the material. Magnetic flux density is always zero inside a superconductor [1].

1.2. Electrical conduction in the theory of superconducting materials

In superconduction there are three basic theories, namely: London, Ginzburg-Landau and BCS Theories. Below are two of them, London and Ginzburg-Landau.

1.2.1. London Theory

Fritz and Heinz London developed a theory that explains the Meissner effect. This effect consists in the fact that the field lines are taken out of a body once it enters the superconducting state.

Using n_s as the density of superconducting electrons and $\mathbf{J_{sc}}$ as the superconducting current density

$$\mathbf{E} = \frac{m}{n_s e^2} \frac{\partial \mathbf{J_{sc}}}{\partial t}, \tag{1.4}$$

which represents the first London equation.
The second London equation is

$$-\frac{m}{n_s e^2} (\nabla \times \mathbf{J_{sc}}) = \mathbf{B}. \tag{1.5}$$

The first characteristic quantity of superconduction is introduced, λ_L (London depth of penetration) and is defined as

$$\lambda_L^2 = \frac{m}{\mu_0 n_s e^2}. \tag{1.6}$$

London depth of penetration values were found to be in the order of 100 nm. Currents are forming on the surface of a superconductor that form a magnetic field which neutralizes any effect that an external magnetic field has inside the superconductor [1].

1.2.2. Ginzburg – Landau Theory

The first equation in GL theory

$$\text{GL I: } \frac{1}{2m^*}\left[\hbar^2\nabla^2\phi - 2i\hbar e^*\mathbf{A}\cdot\boldsymbol{\nabla}\phi - e^{*2}A^2\phi\right] - a\phi - b|\phi|^2\phi = 0. \tag{1.7}$$

The second equation in GL theory

$$\text{GL II}: \ \boldsymbol{\nabla}\times(\boldsymbol{\nabla}\times\mathbf{A}) + \frac{i\hbar e^*}{2m^*}(\phi^*\boldsymbol{\nabla}\phi - \phi\boldsymbol{\nabla}\phi^*) + \frac{e^{*2}}{m^*}\mathbf{A}|\phi|^2 = 0. \tag{1.8}$$

GL theory introduces the length of coherence

$$\xi^2 = \frac{\hbar^2}{2m^*|a|}. \tag{1.9}$$

The ratio $\kappa = \frac{\lambda}{\xi} = \frac{1}{\sqrt{2}}$, also named the G – L parameter, classifies superconductors into two categories [3]

$$\kappa \leq \frac{1}{\sqrt{2}} \qquad \text{(Type I)}, \tag{1.10}$$

$$\kappa \geq \frac{1}{\sqrt{2}} \qquad \text{(Type II)}. \tag{1.11}$$

CHAPTER 2. SUPERCONDUCTING MATERIALS. PROPERTIES

Chapter 2 presents the main types of superconducting materials. Their characteristics and performances, applications of superconducting materials in the field of electrical engineering, manufacturers and specific production methods for each superconducting material, economic impact, advantages and disadvantages are presented.

2.1. Type I and II superconducting materials

Figure 2.1 shows the critical surface of a superconductor depending on its critical parameters: Tc, Bc2 și Jc.

Type I superconductors are elements, while Type II superconductors are made of alloys and composites.

The Type II superconductor is also a perfect conductor of electricity, with zero resistance, but whose magnetic properties are more complex than in the case of Type I superconductors.

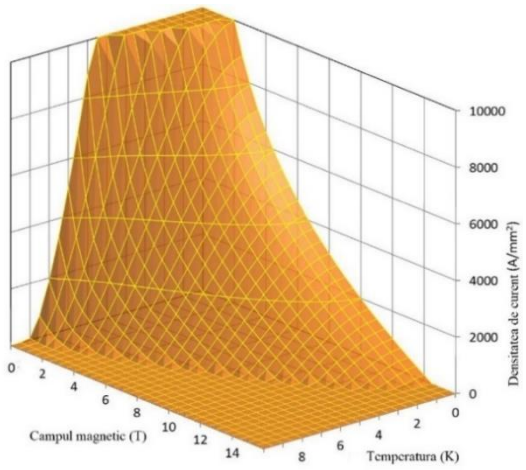

Fig. 2.1. The critical surface of a superconductor.

2.2. LTS superconducting materials

The most widely used LTS superconductor is the ductile alloy of niobium and titanium (NbTi). Due to its superconducting properties, it is suitable for obtaining magnetic flux densities in the range of 2 - 10 T, requiring cooling temperatures below 5 - 6 K (ensured by liquid helium). Another LTS superconducting material which is already produced on an industrial scale is Nb_3Sn.

Cooled to lower temperatures about 18 K, Nb_3Sn becomes superconductor. Nb_3Sn is suitable for obtaining a magnetic flux density in 10 - 21 T and is generally cooled with liquid helium. Nb_3Sn is generally used in the manufacture of the inner coils of nuclear magnetic resonance (NMR) magnets and for the electromagnets in particle accelerators.

2.3. HTS superconducting materials

These materials, generically called high temperature superconductors (HTS), have generated a great deal of interest even outside the scientific community, opening the door to new directions of research and development. The most important HTS materials are Y-Ba-Cu-O, Bi-Sr-Ca-Cu-O and MgB_2.

2.4. HTS materials with practical applicability

2.4.1. Requirements for practical use

HTS materials used for electrical engineering applications have to meet the following minimum conditions, such as conductor length (~ km), high value of current density (~ kA/cm^2), reduced AC losses, structurally stable, low cost / unit length.

2.4.2. Commercially available HTS materials

Commercially available materials are BSCCO-2223, YBCO-123 and MgB_2.

2.4.3. Properties and characteristics of HTS materials

In order for HTS materials to be used in applications, three important features must be taken into account T_C, B_{C2} and J_C.

Regarding the basic characteristics of the main superconducting materials with technical applicability, they are given in Table 2.1.

Table 2.1. Critical parameters of HTS materials with technical applications [9, 11, 12]

No.	HTS Material	T_c [K]	J_c [A/cm^2]	B_{c2} [T]
1	BiSrCaCuO	110	103 – 104@77 K	198
2	YBaCaO	92	104 – 105@77 K	115
3	MgB_2	39	104 – 105@30 K	19-40

2.4.3.1. BSCCO – 2212 conductors

BSCCO-2212 has the critical temperature (T_c) of about 90 K and is interesting primarily for its intense field properties in the temperature range 4,2 – 20 K [4].

2.4.3.2. BSCCO – 2223 conductors

Table 2.2. BSCCO – 2223 band characteristics [4], from AMSC [5], 2006, respectively from SEI [6], 2007

	Parameters	High current density	High mechanical strength
BSCCO – 2223 (AMSC)	The current density [A/cm^2] for I = 150A,	17200	13300
	Average thickness, [mm]	0,21±0,023	0,255±0,0285
	Width, [mm]	3,9 – 4,3	4,2 – 4,4
	Minimum bending diameter [mm]	100	38
	Maximum rated tensile strength [MPa]:		
	- room's temperature	65	200
	- liquid nitrogen temperature (77 K)	65	250
BSCCO – 2223 (SEI)	The current density of a conductor of 150A, [A/cm^2]	15000	12000
	Average thickness, [mm]	0,22±0,02	0,22±0,02
	Width, [mm]	4,2±0,2	4,2±0,2
	Minimum bending diameter [mm]	70	50
	Maximum rated tensile strength, [Mpa]:		
	- room's temperature	100	170
	- liquid nitrogen temperature (77 K)	135	210

2.4.3.3. YBCO-123 type conductors

Table 2.3. Features of 2G copper laminated tape from AMSC, 2010 and Superpower, 2010 [4, 17]

Specifications	Specifications	
	AMSC	Superpower
Minimum I_c [A]	150	80 – 140
Average thickness [mm]	0,2	0,1
Width [mm]	4,83	4
Minimum bending diameter [mm]	30	11
Maximum bending moment [MPa]	150	> 550
Maximum axial relative elongation at 77 K	0,3%	0,45 %
The maximum length of a piece [m]	500	Până la 500

2.4.3.4. Magnesium diboride (MgB_2)

Table 2.4. MgB_2 conductor from Hyper Tech Research [9], 2010.

Parameter	Specifications
Critical current density at 20 K and 2 T	175 kA/cm^2
Superconducting fraction	13 – 18% (30% in the future)
Diameter [mm]	0,7 – 0,9
Number of filaments	7 and 19
Heat treatment / time	700 °C at 20 min
Maximum bending at 77 K	0,35%
The maximum length of a piece [km]	1 – 4

2.5. Applications of HTS superconducting materials

The development of HTS superconducting materials in the form of wires and strips has allowed the approach of industrial applications such as superconducting electric machines, which have increased their efficiency towards 99%.

With higher performance than conventional superconductors, HTS materials have allowed the development of high-performance applications in electrical engineering, such as energy storage systems, electrical cables, motors, transformers and generators. MAGLEV was also developed in rail transport.

CHAPTER 3. THE PHYSICAL MODEL

To describe the operating principle of the EMSD it is necessary to define its physical model. Thus, the simplifying physical hypotheses will be established, the operating regime and the main phenomena that characterize its operation will be identified.

The evaluation of the electromagnetic field and the heat transfer problem are solved using analytical methods and numerical analysis.

3.1. Physical model - the electromagnetic field problem

The laws that define the operating principle of the EMSD and the boundary conditions of the EMSD components constitute its physical model.

3.1.1 The stationary electromagnetic field model in the superconducting electromagnet

The fundamental relations that describe the stationary magnetic field are the following: the magnetic circuit law, the magnetic flux law and the constitutive law for the magnetic field.
The magnetic field in a domain has a unique solution if the following data are known:

- Geometric - data on the shape and dimensions of the domain in question;
- Material data;
- Internal sources in any point in the domain;
- External conditions representing boundary conditions (Dirichlet or Neumann condition).

In stationary form the following mathematical model for the electromagnetic field results

$$\begin{cases} \mathrm{div}\mathbf{B} = 0 \Longrightarrow (\exists)\ \mathbf{A}\ \mathrm{a.\hat{i}.}\ \mathbf{B} = \mathrm{rot}\mathbf{A} \\ \mathrm{rot}(\bar{\bar{\mu}}^{-1}\mathrm{rot}\mathbf{A}) = \mathbf{J} + \mathrm{rot}\left(\bar{\bar{\mu}}^{-1}\mu_0\mathbf{M}_p\right) \end{cases}. \tag{3.1}$$

In a linear environment and with $\mathbf{M}_p = 0$, is obtained

$$\mathrm{rot}(\bar{\bar{\mu}}^{-1}\mathrm{rot}\mathbf{A}) = \mathbf{J}. \tag{3.2}$$

The most important theorems that are deduced from the general and material laws of the electromagnetic field are: general theorems of electromagnetic energy, electromagnetic impulse, general electrodynamic potentials, generalized forces, Maxwellian stresses in electric and magnetic field and volume densities of electric and magnetic forces.

3.2 Heat transfer problem

Between two bodies, the heat transfer is achieved by *thermal conduction, thermal convection* and *thermal radiation*.

Conduction heat transfer

The equation of conductive heat flux is defined by Fourier's law, which characterizes heat transfer by unidirectional thermal conduction through a material with a thermal conductivity [28]

$$q_x \overset{\text{def}}{=} -k\mathbf{grad}T, \tag{3.3}$$

where k [W/mK] is the thermal conductivity of the substance and T [K] is the temperature.

Convection heat transfer

Convection heat transfer is described by Newton's law [28]

$$q''_{\mathrm{conv}} \overset{\text{def}}{=} h(T_w - T_\infty), \tag{3.4}$$

where T_w [K] represents the surface temperature of the solid body, T_∞ [K] is the free stream temperature, q''_{conv} [W/m^2] is the convection heat flux and h [W/m^{2}K] is the convection heat transfer coefficient.

Radiation heat transfer

The radiative heat flux emitted by a real surface, the so-called gray surface, is only a fraction of that emitted by a black body [28]

$$q''_{SB,b} = \varepsilon\sigma T_S^4, \tag{3.5}$$

where T_S is the absolute temperature of the body surface, σ is Stefan-Boltzmann constant ($\sigma = 5.67 \times 10^{-8}$ W/m^{2}K) and ε is the emissivity.

CHAPTER 4. DESIGNING THE EMSD EXPERIMENTAL MODEL

This chapter presents the stage preceding the magnetic design of an EMSD prototype, a "conceptual" model, which can generate a magnetic field with magnetic flux density of maximum 3 T and uniform (~ 10^{-3}) in the area of interest that is located in the "hot channel" of the EMSD.

4.1. HTS electromagnet overview

The experimental model of EMSD has the structure indicated in Fig. 4.1:

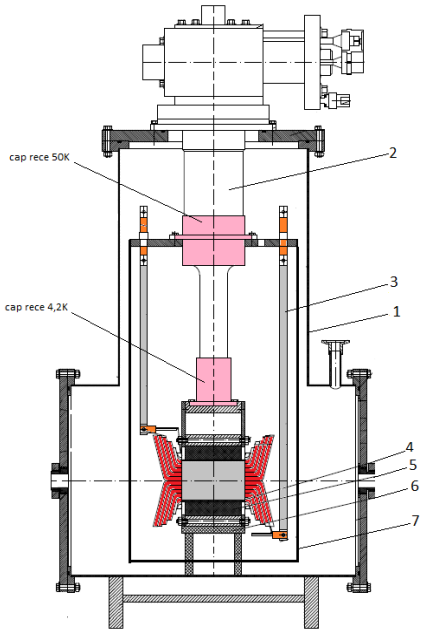

HTS electromagnet structure:

1. Cryostat;
2. Cryocooler;
3. HTS conductors;
4. Superconducting winding;
5. Yoke;
6. Insulating support;
7. Thermal shield.

Fig. 4.1. Experimental model of HTS electromagnet.

4.2. EMS conceptual model

4.2.1. General characteristics

In order to function as a deflector magnet, the electromagnet meets the requirements summarized in the Table 4.1.

Table 4.1. Imposed characteristics of the electromagnet

Parameter	Specifications
The magnetic flux density	2 - 3 T
Non-uniformity of the magnetic field (definition)	~ 10^{-3}
Inner channel diameter	20 mm
Useful volume of the magnetic field	15 cm^3
Cooling type / mode	Contact / Cryocooler
Superconducting material	HTS type
Vacuum level	10^{-3} – 10^{-5} torr

4.2.2. Description of the EMSD Conceptual Model

Taking into account the constraints and requirements imposed, the EMSD conceptual model has been developed and is presented schematically in Fig. 4.2.

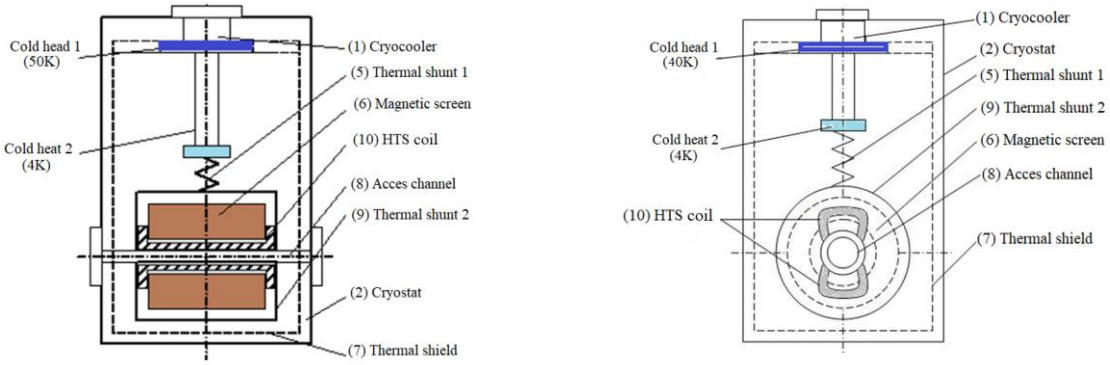

a) Cross-longitudinal section. b) Transversal – axial section.

Fig. 4.2. Conceptual model of HTS dipole electromagnet.

4.3. Superconducting coils

Using numerical modeling that allowed the evaluation of the magnetic field generated by the electromagnet, the number of coils, their configuration and the number of turns required for each coil were determined so that the desired magnetic field could be generated (Table 4.2).

Table 4.2. Characteristics of superconducting coils

HTS coil	Coil thickness [mm]	No. of turns
1	13.5	75
2	12.5	69.4
3	11	61
4	9.5	53
5	7.5	42
6	5.0	28
7	2.5	14

4.4. Cryogenic cooling system

This cooling system of the electromagnet has as main component the Gifford - McMahon cryocooler, thus eliminating the use of cryogenic agents. The cryocooler type is a closed cycle one, with two cooling stages (50 K and 4,2 K). A RDK 415D cryocooler was used, purchased from Sumitomo [30].

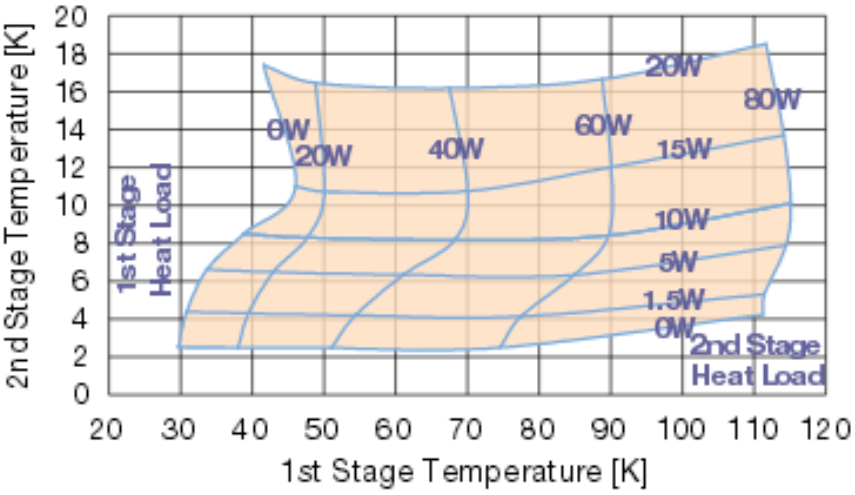

Fig. 4.3. Functional characteristic of the RDK-415D cryocooler [30].

4.5. Characteristics of HTS current conductors

In the design of HTS current conductors, functional parameters were taken into account, such as the maximum supply current of the HTS coils and a reduced heat transfer to the HTS electromagnet.

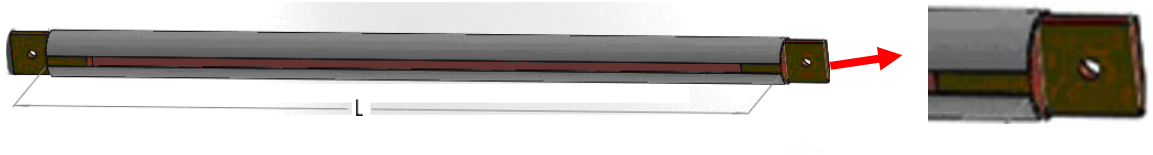

Fig. 4.4. HTS conductor.

CHAPTER 5. DESIGNING USING NUMERICAL MODELING OF DIPOLE SUPERCONDUCTING ELECTROMAGNET

5.1. Current status

Superconductivity has many applications of interest in medicine, science, energy systems, transportation and electronics. One of the most important applications of superconductivity are superconducting electromagnets, for example electromagnets for NMR, MRI, electromagnets for particle accelerators and electromagnets for nuclear fusion. Most of these applications still use low temperature superconducting materials (4,2 K – 30 K).

5.2. Superconducting dipole electromagnet

The structure of the dipole superconducting electromagnet (EMSD) is as follows:

1. Electromagnet cryostat constructed of non-magnetic stainless steel (austenitic).
2. Gifford - McMahon cryocooler RDK - 415D with two temperature levels at 50 K and 4,2 K.
3. HTS current conductors from HTS superconducting material of YBCO type.
4. HTS coils of YBCO superconducting tape and impregnated with low temperature epoxy resin.
5. Iron yoke made of carbon steel OL.
6. Electromagnet support made of DurAl.
7. 50 K thermal shield made of polished copper sheet.

HTS coils are made in the shape of a saddle, except for two of them, which have the shape of a racing circuit. A total of 10 coils are interconnected to generate an uniform magnetic field with magnetic flux density of 2,5 T.

5.3. Design and numerical modeling of EMSD - magnetic field

Due to iron saturation, an uniform magnetic field winding produced by an iron coreless electromagnet will be used. (Fig. 5.1).

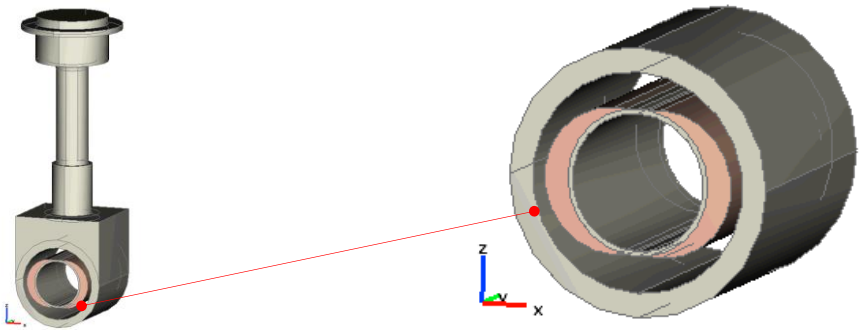

a) The cryostat - magnet subassembly. b) HTS coil for uniform field.

Fig. 5.1. CAD model of HTS electromagnet for uniform field.

5.3.1. Uniform field excitation winding

The analysis of the magnetic field problem is performed for a representative 2D model, respectively in the median plane of the electromagnet (a cross section plane, perpendicular to the *Oy* direction from Fig. 5.1).

The stationary model of the magnetic field for linear media in the HTS electromagnet is described by the partial derivative equation [44]

in the winding

$$\nabla \times (\mu_0^{-1}\mu_r^{-1}\nabla \times \mathbf{A}) = \mathbf{J}, \tag{5.1}$$

outside the winding

$$\nabla \times (\mu_0^{-1}\mu_r^{-1}\nabla \times \mathbf{A}) = 0, \tag{5.2}$$

where **J** [A/m^2] is the density of the electric current in the windings, **A** [T/m] is the magnetic potential vector, $\mu_0 = 4\pi\times10^{-7}$ H/m represents the magnetic permeability of the vacuum and μ_r is the relative permeability. The boundary condition that completes the magnetic field problem is magnetic insulation, respectively **n** × **A** = 0, where **n** is the outside normal component at the computational domain.

5.3.2. Analytical model for the calculation of the magnetic field

In a first stage, the excitation solenation is approximated by an equivalent current web, $J_s = J_0 \cos\alpha$, where α is the angle at center (Fig. 5.2 b). In Fig. 5.2 the magnetic flux density in the considered domain is presented, highlighted both by field lines and by arrows. In case of $J_0 = 2{,}5\cdot10^6$ A/m, a magnetic field is obtained in the *y* direction with a magnetic flux density value equal to B_y = 3,124 T.

In the solving stage of the problem that for the distribution of the solenation as a current web considers the equations (5.1) – (5.2), numerical analysis based on the finite element method was used [45].

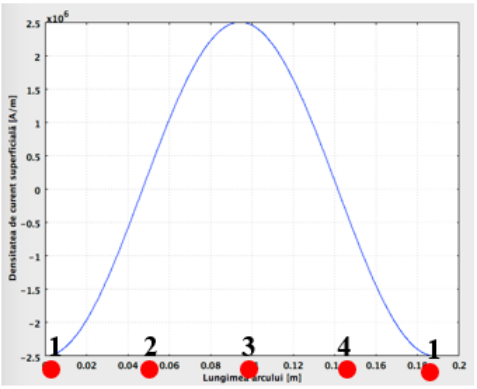

a) Excitation solenation approximated with a current web.

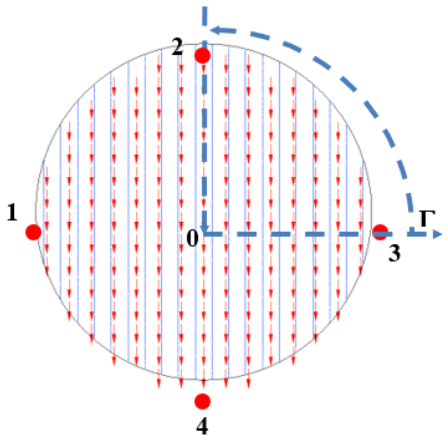

b) Magnetic flux density, B_y = 3,142 T.

Fig. 5.2. Winding for uniform magnetic field - the solenation is distributed harmoniously.

The magnetic circuit law applies to the named contour Γ (Fig. 5.2.b), $Arc(P_3P_2)\to\infty$

$$n \cdot i = \oint_\Gamma \mathbf{H}\cdot\mathbf{d}\,\mathbf{r} = \int_{P_2}^{P_0} \boldsymbol{H}\,\mathrm{d}\,z = \boldsymbol{H}r = \int_0^{\pi/2} JA_{amp}\cos\theta\, r\,\mathrm{d}\,\theta = JrA_{amp}, \tag{5.3}$$

where *i* [A] represents the intensity of the electric current through a coil, *n* represents the number of turns, **H** [A/m] represents the intensity of the magnetic field (vertical component) and A_{amp} [m] represents the "amplitude" of the winding thickness (which is measured in the radial direction, at α = 0).

5.3.3. Numerical model for magnetic field evaluation

Figure 5.3 shows the numerical solution of the magnetic field problem by color map and field lines for magnetic flux density. In these circumstances, B ~ 2,303 T and $J = 3 \cdot 10^8$ A/m^2 for n = 250 turns.

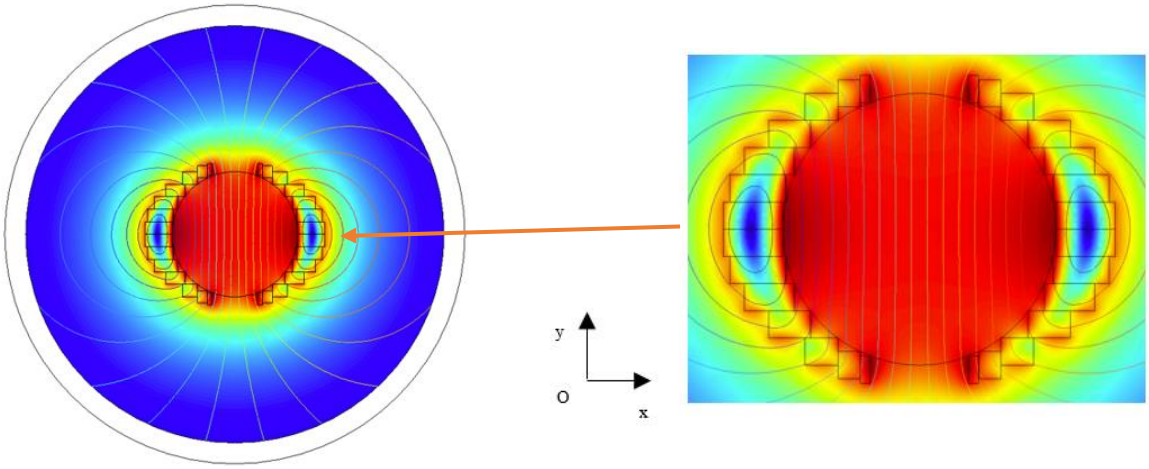

a) Magnetic flux density. b) Magnetic flux density – detail.

Fig. 5.3. Representation of the magnetic field in the HTS type solenoid with cosine winding, B_{max} = 2,3 T; the dimensions are in mm.

5.4. Design using numerical modeling of EMSD - electrodynamic forces - 2D

Laplace-type forces act on the coils [44]

$$\mathbf{f} = \mathbf{J} \times \mathbf{B}, \tag{5.4}$$

where $\mathbf{f}$ [N/m^3] represents the force density. Using the numerical solution of the stationary magnetic field problem, $\mathbf{f}$ distribution is determined.

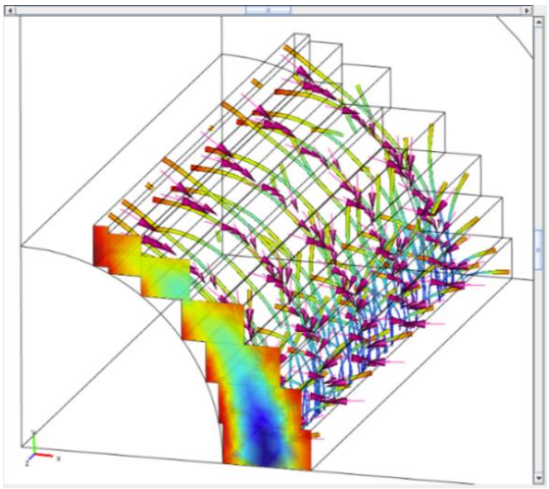

Fig. 5.4. Electrodynamic force density distribution, acting on HTS coils, represented by field tubes, color map and arrows - the maximum value is $6{,}08 \cdot 10^8$ N/m^3.

Figure 5.4 presents the distribution of the electrodynamic forces density (Laplace) which is acting on the sides of the coils traversed by current and located in the magnetic field (own), solution of the 3D magnetic field problem.

5.5. Evaluation of the electrodynamic forces produced by the magnetic field of EMSD - 3D

As already mentioned, the aim is to design and simulate a superconducting dipole electromagnet, intended to generate an intense magnetic field (~ 2,5 T) and with a high uniformity (10^{-3}) in the central region of the electromagnet called the "appropriate field area" (GFZ).

5.5.1. Identification of the areas most required by electrodynamic forces

The following expression was used to calculate the Laplace force

$$\mathbf{F} = \frac{1}{\mu_0}\int_V [(\boldsymbol{\nabla} \times \mathbf{B}) \times \mathbf{B}]\mathrm{d}V, \tag{5.5}$$

where **F** [N] represents the resulting Laplace force and V [m^3] is the volume of the winding.

In this problem the electric field source is on the boundary (remote cross section, through coil, Fig. 5.5). A current density of 10^7 A/m^2 is assumed.

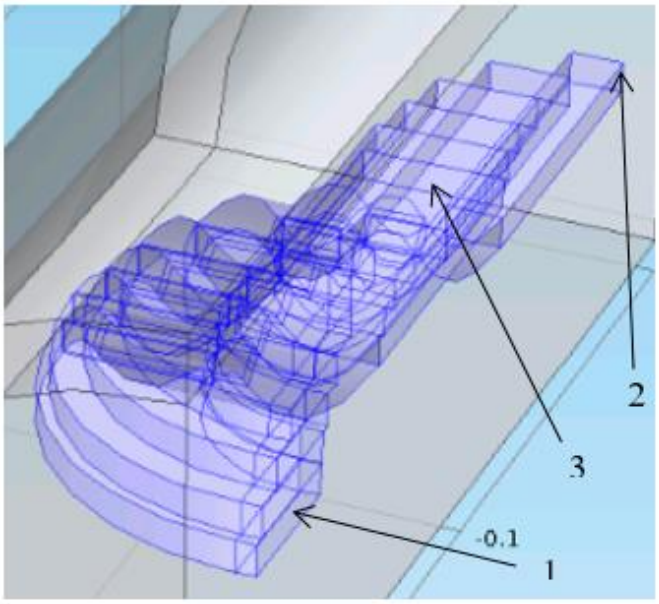

Fig. 5.5. Reduced numerical model - detail.

Next, using the Laplace forces thus determined, the mechanical stresses are calculated and are presented in Fig. 5.6.

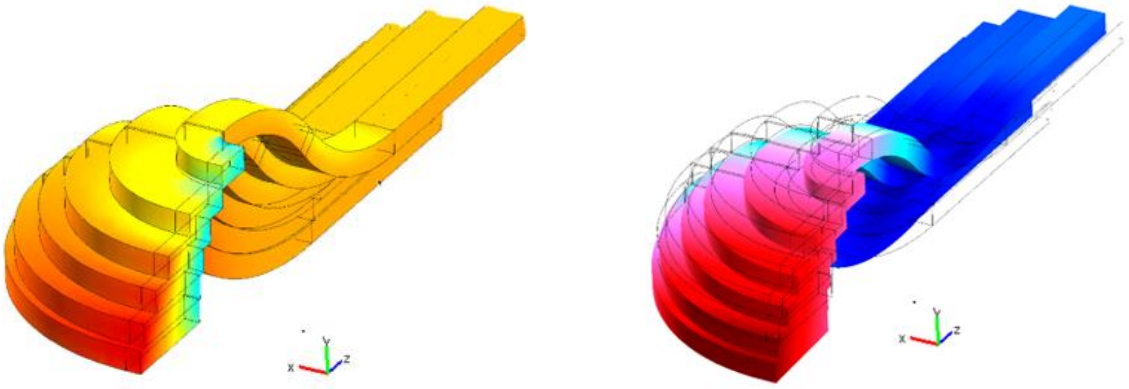

a) *Oz c*omponent, Laplace force, maximum value $8 \cdot 10^6$ N/m^2.

b) The maximum deformation is 8,2 μm.

Fig. 5.6. Numerical simulation results for the structural problem.

5.5.2. Evaluation of deformations that may occur in EMSD, following the action of electrodynamic forces

The deformation of the coil windings due to the electrodynamic forces is influenced by the mechanical support on which they are fixed. In the present study, three cases were analyzed (Fig. 5.7, the case with the most important deformation).

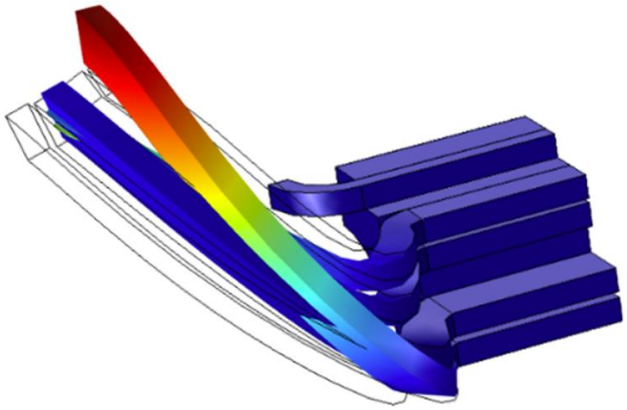

Fig. 5.7. Deformations generated by electrodynamic forces. The hot channel is the only fixed part, maximum deformation value 0,0293 m. The hot channel is the point of support. Values are expressed in meters. Distortions are magnified 5,000 times for better viewing.

In this study the basic properties were used (Young's module E = 113 GPa, Poisson's coefficient ν = 0,1, mass density ρ = 6,3 g / cm^3) [48].

5.6. Design and numerical modeling of EMSD - heat transfer

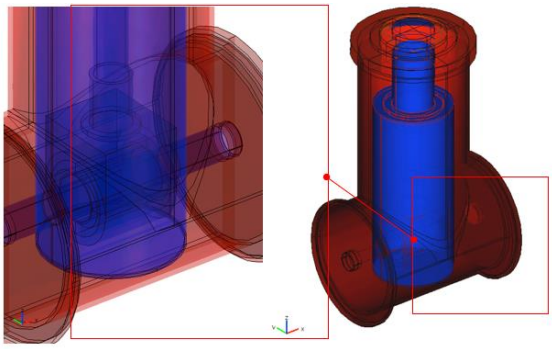

Fig. 5.8. Temperature distribution in the cryostat system and HTS type electromagnet, T_{max} = 278 K.

Figure 5.8 shows the temperature field in the considered domain (colors are proportional to the local temperature) considering a h = 2 W/m^{2}K.

Table 5.1. Numerically and analytically estimated thermal loads

Cooling stage	Thermal power [W] Numerical analysis	Thermal power [W] Analytical calculation
2nd cold room (stage 2), 50 K	15,76	16,35
First cold room (stage 1), 4 K	6,94	7,65
Heat transfer from the outside, T_{medium} = 293,15 K (Total thermal load)	22,70	24

The values in Table 5.1 are verified experimentally.

5.6.1. Analytical calculation of the thermal loads produced by the system (supported by the cryocooler)

Conductive thermal fluxes in solid elements

The integral of the thermal conductivity was calculated having as reference the temperature of 4 K, $\int_{4K}^{T_2} k(T)dT$, for the most commonly used materials in the manufacture of cryostats

$$\dot{q}_{cond} = \frac{A}{L}\int_{T_1}^{T_2} k(T)dT = \frac{A}{L}\left\{\int_{4K}^{T_2} k(T)dT - \int_{4K}^{T_1} k(T)dT\right\}, \quad (5.6)$$

where A [m^2] is the cross-sectional area, L [m] is the length; T_1 and T_2 are the temperatures at the ends of the element (HTS current conductors).

Radiative thermal fluxes (cryostat-thermal screen, thermal screen - electromagnet)

The radiative heat flux was calculated using the following formula [50]

$$q_r = \varepsilon_r \sigma (T_{hot}^4 - T_{cold}^4). \quad (5.7)$$

The thermal loads analyzed analytically are verified by the results obtained through numerical modeling, respectively obtained experimentally (Table 5.1).

5.7. Numerical modeling of superconducting junction operation

In Fig. 5.9.a), the magnetic field is represented by magnetic flux density field lines.

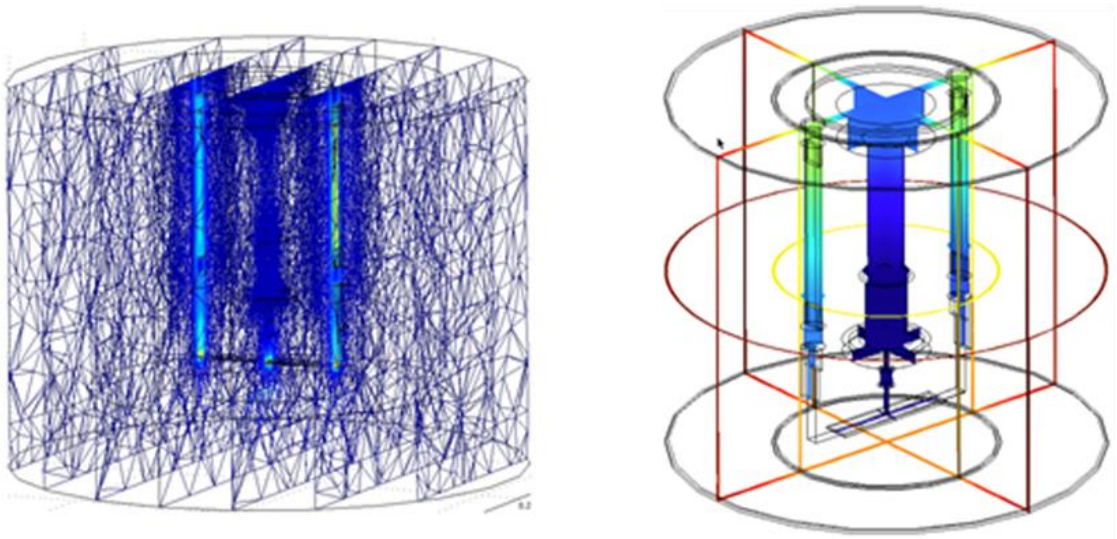

a. b.

Fig. 5.9. Magnetic flux density represented by field lines, maximum value 0,03 T (a) and temperature distribution - values are in Kelvin degrees, between 4,2 K and 292 K (b).

The heat transfer problem was also solved using the FEM technique. Linear Lagrange elements were used to integrate a nonlinear scalar field problem.

Table 5.2. Thermal loads extracted by the cryocooler G-M

Cooling stage	Thermal load [W]
I (50 K)	30,70
II (4,2 K)	3,76

Table 5.2 shows the thermal loads to be extracted from the system, using the cryocooler.

CHAPTER 6. DEVELOPMENT OF EXPERIMENTAL MODEL FOR EMSD

6.1. Development of the experimental model

Next, the development of the main components of the superconducting electromagnet system will be presented so as to obtain the parameters initially imposed. [53].

A. Superconducting coils

There are two constructive types of coils: "stadium" and "saddle".

Fig. 6.1. HTS stadium type superconducting coils.

Fig. 6.2. HTS superconducting coils of the "saddle" type.

B. Coil support

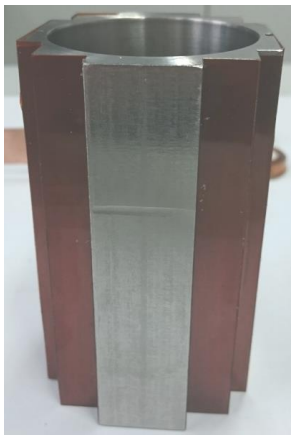

Fig. 6.3. HTS coil support.

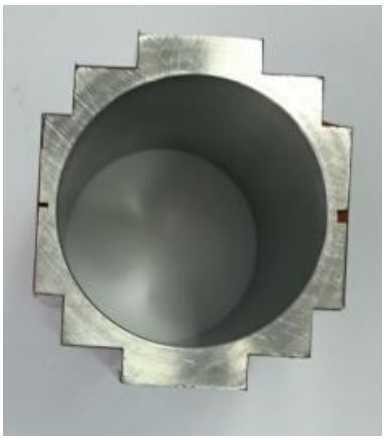

Fig. 6.4. Section view of the coil holder.

Fig. 6.5. Coil assembly and their support.

The support of the coils (Fig. 6.3, 6.4.) has the role of supporting the assembly (Fig. 6.5.) and maintaining their fixed position in the appropriate locations, to ensure the generation of an uniform dipole magnetic field.

Fig. 6.6. Thermal shunt.

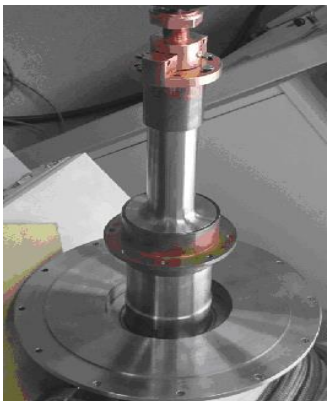

Fig. 6.7. Thermal shunt assembled on the cryocooler.

C. The thermal shunt

It is made of solid copper, for maximum thermal conduction (Figs. 6.6, 6.7).

D. Magnetic screen (iron yoke)

Its role is to close the magnetic field lines and contribute to the uniformization of the magnetic field.

Fig. 6.8. HTS coils and yoke, axial - front view.

E. Thermal shield

Its role is to protect the superconducting coil and the cold head (4,2 K) of the cryocooler from the thermal radiation coming from the cryostat housing (Fig. 6.9).

Fig. 6.9. Thermal shield of the electromagnet.

E. The cryostat

The cryostat is made of non-magnetic stainless steel (austenitic) in a geometry with biaxial symmetry. The main components of the cryostat are shown in Figs. 6.10 and 6.11. The cryostat has a main body (1) and three closing flanges (2). As the electromagnet operates in a vacuum environment, the cryostat must be vacuumed through a vacuum coupling (3) connected to the

external vacuum pump. The power supply of the electromagnet is made by means of two current passes (4), and for the monitoring and testing of the electromagnet, a plug for electrical signals (5) is used, which takes the signals given by the sensors and transmits them to the measuring devices.

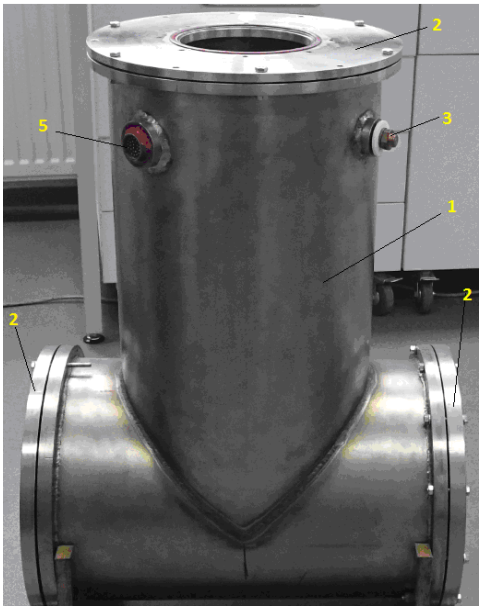

Fig. 6.10. Cryostat side view.

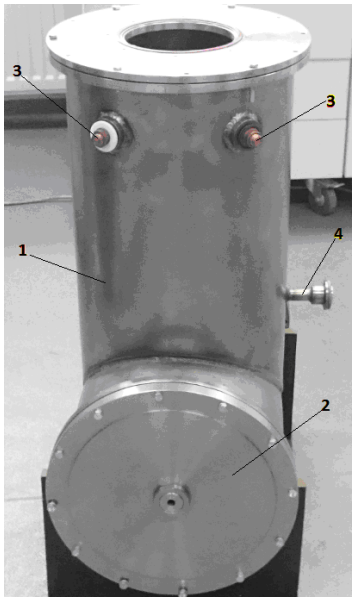

Fig. 6.11. Cryostat front view.

F. The cryocooler

The cryocooler (Fig. 6.12) is a heat pump that works in two cooling stages.

Fig. 6.12. Gifford-McMahon RDK-415 D two-stage cooling cryocooler.

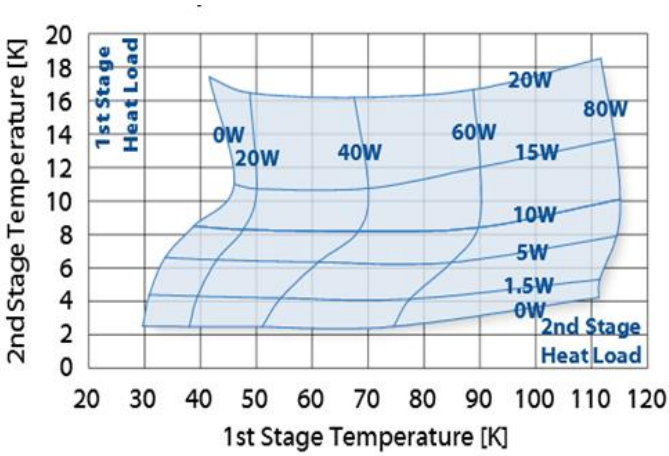

Fig. 6.13. Operating characteristic of the cryopooler RDK-415 D [3].

H. Current conductors

These current conductors supply the superconducting coils to relatively high currents (~ 200 A).

Fig. 6.14. HTS conductors with Cu-HTS junctions at the ends.

Fig. 6.15. HTS conductors assembled in housings.

Fig. 6.16. Copper conductors together with the cryocooler.

6.2. Assembling the experimental EMSD model

All constituent components of the dipole superconducting magnet were assembled in the cryostat and coupled to the cryocooler (Fig. 6.17).

c. Cryostat - coils - thermal shield assembly, mounted in cryostat.

d. Assembled dipolar superconducting electromagnet (EMSD).

Fig. 6.17. Dipolar superconducting electromagnet assembly.

The system thus assembled (Fig. 6.17) was preliminarily tested on subassemblies (vacuum and cooling tests at cryogenic temperatures, verifying the entrance in superconduction of the superconducting coils) and then subjected to final operating tests by power supply from a direct current source.

CHAPTER 7. TESTING THE SUPERCONDUCTING ELECTROMAGNET

To establish the experimental functional parameters of EMSD, experimental assemblies were made for measuring the critical current of the superconducting tape, of the individual superconducting coils at liquid nitrogen temperature, of the generated magnetic field and the uniformity of the magnetic field generated by the HTS electromagnet, of the HTS / HTS and HTS / Cu junctions electrical resistances. These assemblies and the results obtained are described below.

7.1. Tests and experiments performed on EMSD

Preliminary tests aimed to verifying experimentally the necessary conditions for the proper operation of the assembly: the vacuum level in the cryostat and the operation of the cryocooler, as well as measuring the critical currents of the HTS coils of the magnetic field generated by EMSD in its center, uniformity of the generated magnetic field.

7.1.1. Testing vacuum conditions in cryostat

An EDWARDS turbomolecular pump vacuum system was used to vacuum the superconducting magnet assembly (cryostat) [55], with a capacity of 50 l / min and a final pressure of 10^{-8} mbar, as can be seen from Fig. 7.1.

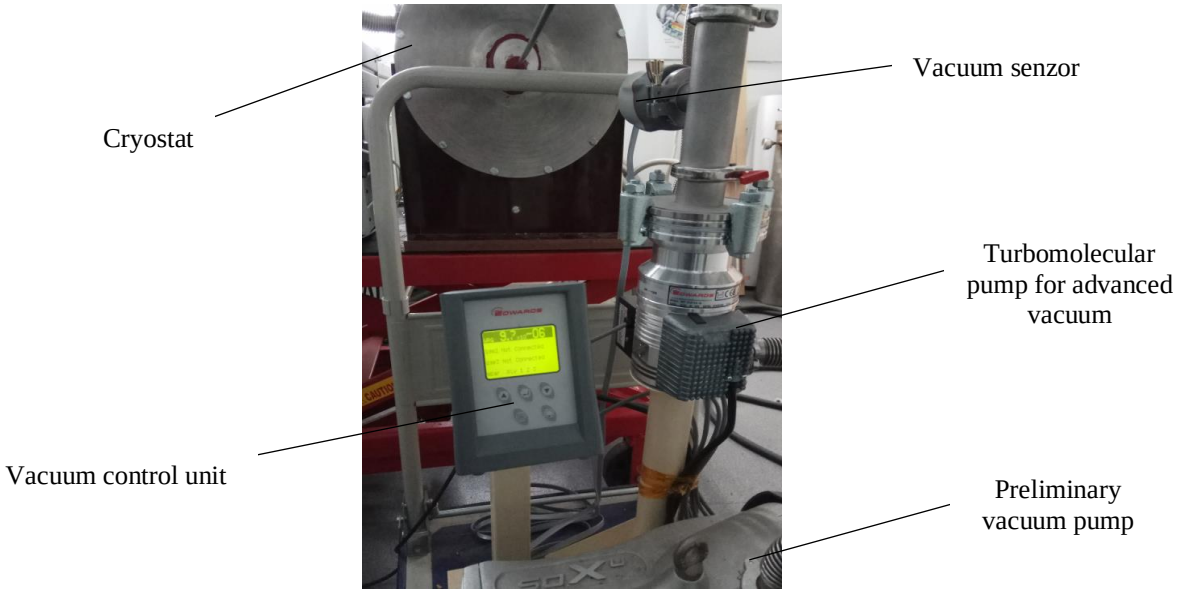

Fig. 7.1 EMSD electromagnet cryostat vacuuming.

The working pressure in the cryostat was 10^{-6} mbar.

7.1.2. Testing the functional parameters of the cryocooler

The cryocooler is RDK-D415 type, a product of SHI-Cryogenics [30]. The functional characteristic of this cryocooler is presented in Fig. 7.2.

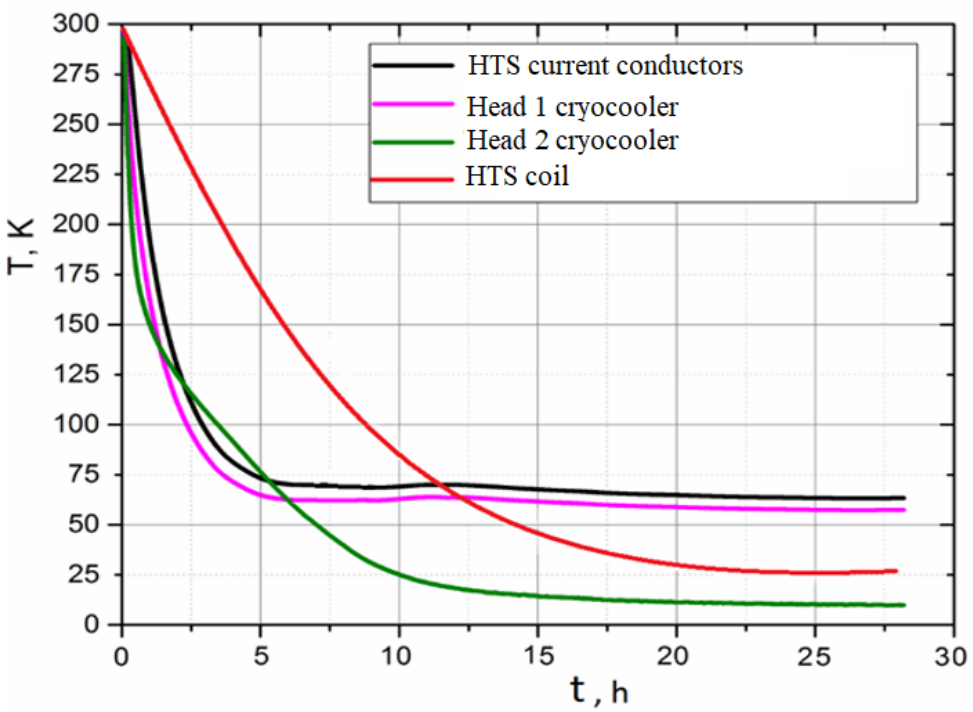

Fig. 7.2. HTS dipole magnet cooling tests with RDK 415D cryocooler.

7.1.3. Measurement of the characteristic parameters of the superconducting coils

Eight superconducting coils were made, the number of turns and electrical parameters of which are shown in Table 7.1.

Table 7.1. HTS superconducting coils parameters

Coil no.	No. of turns	Electrical resistance [Ω]	Inductivity [H]
1	56	3,095	$1{,}15 \cdot 10^{-3}$
2	56	3,017	$1{,}10 \cdot 10^{-3}$
3	73	3,94	$1{,}80 \cdot 10^{-3}$
4	68	3,41	$1{,}36 \cdot 10^{-3}$
5	68	3,715	$1{,}59 \cdot 10^{-3}$
6	73	4,43	$2{,}28 \cdot 10^{-3}$
7	38	0,9123	$0{,}21 \cdot 10^{-3}$
8	38	0,94125	$0{,}22 \cdot 10^{-3}$

The temperature at which the measurements were performed in the laboratory was 25°C.

Critical current measurement system

The principle scheme of the experimental assembly used for measuring the critical current of the superconducting coils is presented in Fig. 7.5.

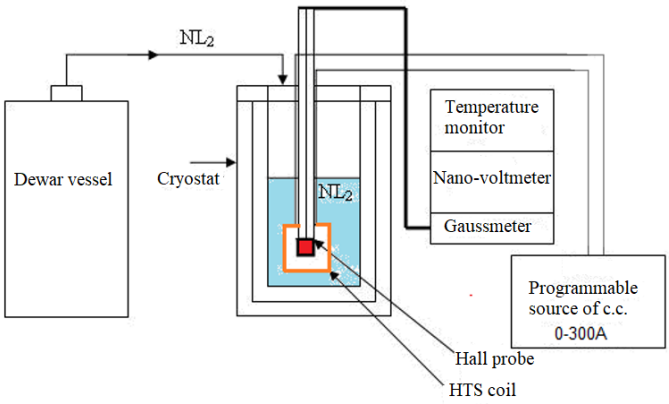

Fig. 7.3. Schematic of the critical current measurement assembly for superconducting coils.

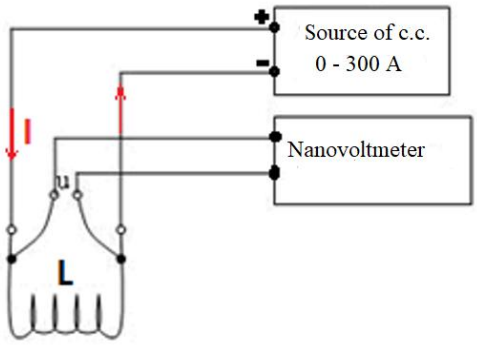

Fig. 7.4. The principle of the measurement method.

The critical current (I_c) was determined using the 4-point measurement method (Fig. 7.4.), the connections being made directly on the measuring sample (Fig. 7.5).

Using the same method, the critical current of the 6 mm wide HTS superconducting tape at 77 K was determined experimentally, the result being presented in the graph in Fig. 7.6.

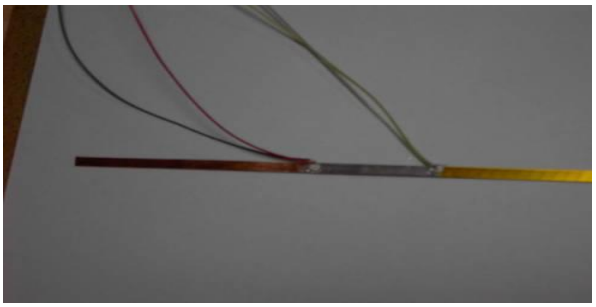

Fig. 7.5. Voltage connections on the HTS superconducting sample.

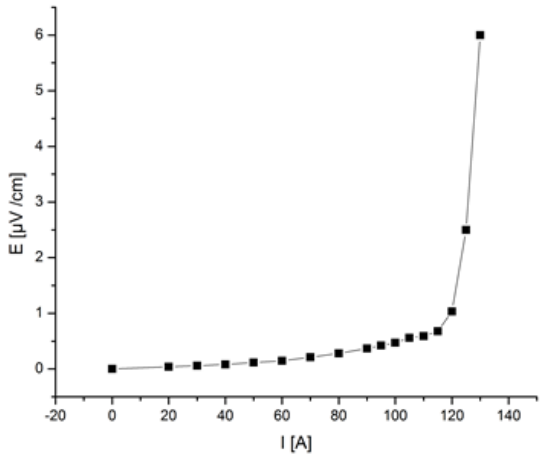

Fig. 7.6. Critical current for HTS superconducting tape, YBCO type.

Table 7.2. Critical currents of HTS coils in its own magnetic field

Coil no.	I_c [A] at 77 K	B‖S (f_a = 6)	B ⊥ S (f_a = 3)
		$I_c \cdot f_a$	$I_c \cdot f_a$
1	110	660	330
2	72	432	216
3	70	420	210
4	75	450	225
5	115	690	345
6	75	450	225
7	84	504	251
8	75	450	225

Thus, in the presence of the magnetic field and at a reference temperature of 20 K, for the superconducting coils of the dipole magnet, are the following values of the critical current, correspondingly multiplied by the so-called "amplification factor" – f_a considered both for B||S and B⊥S, for 2,5 T, considered to be the highest value of the magnetic flux density (Table 7.2).

7.1.4. Magnetic field measurement generated by EMSD

Connecting the programmable direct current source (Fig. 7.7) which can generate max. 300 A at the external terminals of the electromagnet (EMSD), allows its supply and the generation of dipole magnetic field.

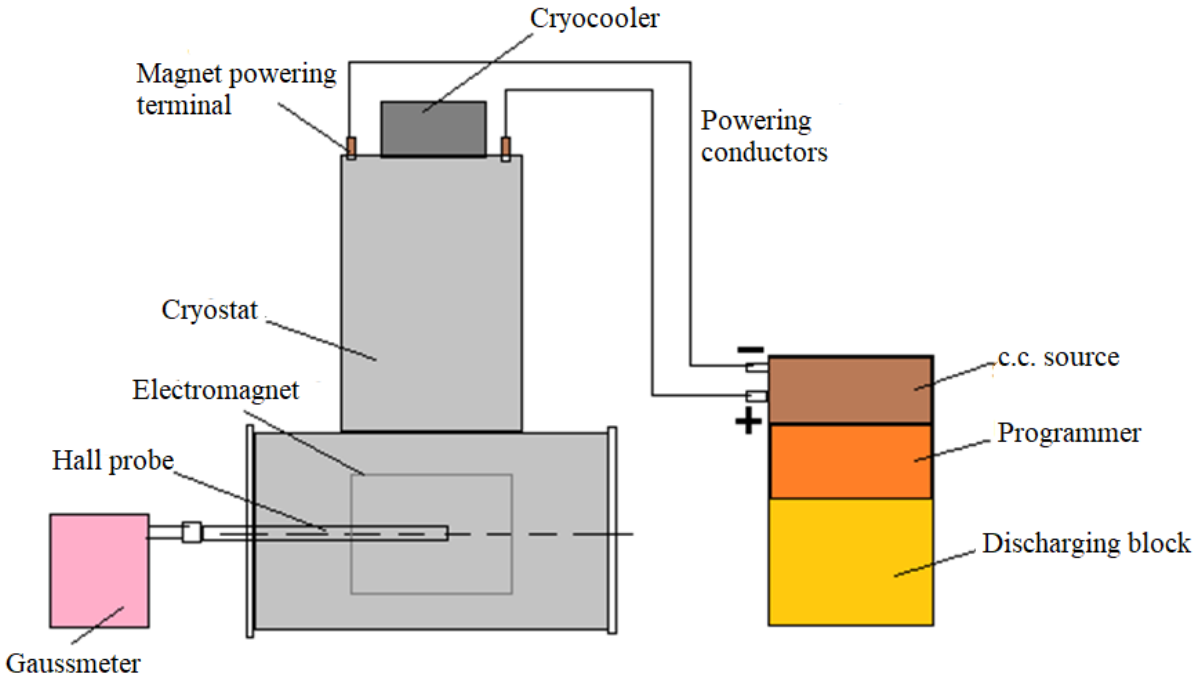

Fig. 7.7. Schematic of the supply and measurement of the magnetic field generated by the HTS electromagnet.

Figure 7.8 shows the experimental set for measuring the magnetic field.

Fig. 7.8. EMSD assembly and magnetic field measurement system.

The generated field was measured in the center of the electromagnet. The results are plotted in Figs. 7.9 and 7.10.

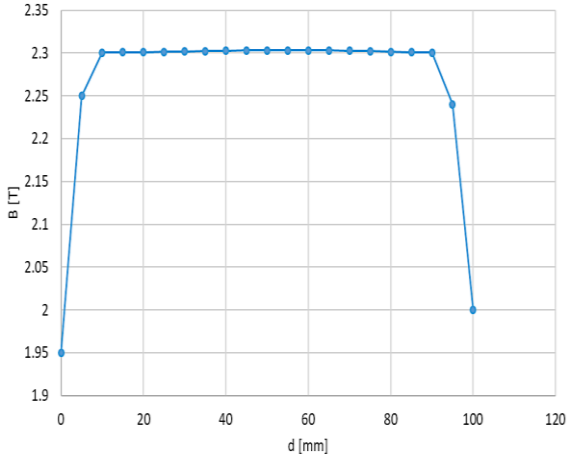

Fig. 7.9. The magnetic field generated by EMSD on the geometric axis of the magnet.

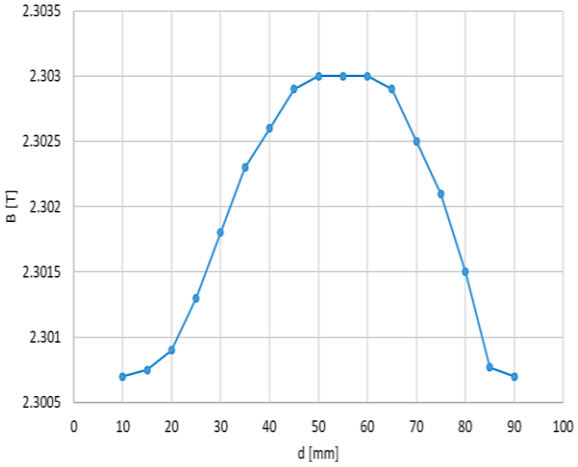

Fig. 7.10. Uniformity of the magnetic field measured on the geometric axis of the EMSD.

Figure 7.23 shows the non-uniformity of the magnetic field measured along the geometric axis of the magnet from which results a maximum non-uniformity of approximately 0,1% considering the magnetic field area measured between 10 - 90 mm.

7.2. Junctions experimental measurement

In the first phase, the resistance of the junctions at liquid nitrogen was determined experimentally, (77 K), results presented in Table 7.3.

Table 7.3. Junction resistance measured at 77 K

Junction type / solder alloy	Electrical resistance [μΩ]
Cu-HTS/SnPb	11,50
Cu-HTS/InAg	5,88
HTS-HTS/SnPb	0,44
HTS-HTS/InAg	0,55

It is observed that the best values obtained are for Cu - HTS using an InAg solder alloy, while for HTS - HTS, the best values were obtained using SnPb solder alloy.

The second experimental phase was the testing of the junctions, using the experimental model presented in the previous subchapter.

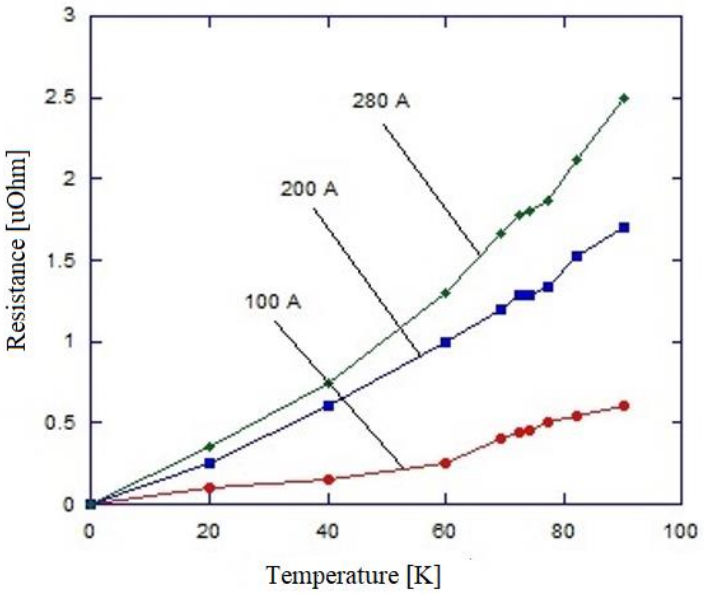

Fig. 7.11. Dependence of the HTS - HTS junction resistance as a function of temperature, at different currents.

CONCLUSIONS

C.1. General conclusions

Chapter 1 presents general theoretical aspects that make the connection between the classical theory and that of superconducting materials, in electrical engineering.

The production of high-performance and affordable MgB_2, BSCCO and YBCO superconducting materials which has led to the development of industrial-scale applications, are presented in Chapter 2. Superior to conventional superconductors, HTS materials have allowed the development of high-performance applications in electrical engineering, such as: electric machines, electromagnets, energy storage, electric cables. Also, in railway transport, the MAGLEV was developed, the high-speed train with magnetic suspension, which greatly increased

the travel speed: at about 500 km / h. The relatively small number of applications is due to their current high cost.

The use of HTS superconducting materials, which have high performances in terms of critical current and transport capacity and in developing various applications, has made the mass and volume of devices made on their basis, be greatly reduced. Thus, devices based on HTS materials were reduced to about 1/2 of the mass and 1/3 of the volume of similar conventional devices (2005 year level figures).

This paper represents the current international trend in this field, which includes other specialized laboratories from other countries, namely to make applications in the field of superconducting electromagnets with new HTS materials. Thus, the stake is both to increase their performance (obtaining intense magnetic fields over 15 T) and to substitute conventional superconducting electromagnets through replacing cooling with liquid helium, liquid nitrogen or cryocoolers, which would significantly reduce their operating costs.

Chapter 3 is the starting point in establishing a mathematical model for the dipole superconducting electromagnet that was designed in Chapter 4 and modeled numerically in Chapter 5.

Chapter 4 of the paper presented the design elements of the experimental EMSD model, together with the main characteristics of the various component elements.

For the EMSD development, a sinusoidal configuration was chosen for the distribution of the solenation, consisting of 7 + 7 HTS coils. The windings were designed and made in the form of a "saddle", mainly, and in the form of a "stadium" the rest.

HTS current conductors have been designed and made to conduct a maximum current of 300 A at a temperature of 77 K, which is why they have been made of 12 mm wide HTS tape.

The chosen cryocooler is of the G-M type with two cooling levels: level 1 at 50 K and level 2 at 4,2 K.

Chapter 6 of the paper presents constructive elements of EMSD, as they were made in the Applied Superconductivity Laboratory of ICPE-CA. The following critical components were made and assembled: the electromagnet cryostat, the cryocooler, the HTS coils, the iron yoke, the HTS current conductors, the electromagnet support and the thermal shield. With the exception of the cryocooler produced by Sumitomo (ShiCryogenics), Gifford-McMahon type, all other components of the EMSD were made, tested and assembled in the Applied Superconductivity Laboratory.

C.2. Original contributions

The doctoral thesis ***„Studies concerning an HTS superconducting electromagnet for intense and uniform magnetic field”*** is a theoretical and practical approach to the use of high temperature superconductors (HTS) in making a dipole superconducting electromagnet, by conducting specialized studies, designing, making and testing superconducting coils with special characteristics, which are part of a superconducting dipole electromagnet (EMSD), while

presenting the advantages of using HTS materials in the field of electrical engineering. The main fields in which these specific applications are found are: electric machines, medicine (MRI, CT), research laboratories or high energy physics.

The original contributions of the thesis are:

- A synthesis of the properties and parameters of HTS superconducting materials and their applications in research and industry, with a focus on the production of intense magnetic fields.
- Participation in the design and production of HTS coils with special shapes that are part of a superconducting electromagnet. Due to the special development conditions (nature of the material, conditions of use and special shape of the saddle type) the design algorithm was modified so as to correspond to the new criteria.
- The experimental study of the critical parameters of HTS materials (T_c, I_c), as well as the critical current of HTS coils, coil cooling duration etc. These studies highlighted a maximum current of 115 A, which can be supported by HTS material. The U – I dependence proved to be similar to that of the literature, namely, linear and increasing.
- To be measured, the HTS coils were cooled with liquid nitrogen. The measurement of the critical current showed a linear characteristic of the voltage at the coils terminals, depending on the supply current. The optimum operating current of the HTS superconducting coils was also determined. The critical current for the coils was determined using the criterion of 1 μV / cm (according to international standards), thus establishing the maximum operating current for the superconducting electromagnet.
- Implementation of an analytical and a numerical model for the calculation of the magnetic field generated by the superconducting electromagnet, results verified also by experimental data obtained in the laboratory.
- Implementation of a thermal numerical model of the entire cryostat - magnet assembly which is verified by an analytical model for the calculation of thermal loads that occur in the system.
- Implementation of a numerical model for the design and testing of superconducting junctions, important elements in the structure of the entire cryostat - magnet assembly.
- Implementation of a numerical model for the evaluation of Laplace forces, identification of areas where these forces are strongest and thus measures could be taken to prevent damage to the electromagnet.
- Participation in the design, realization and testing of a dipolar HTS superconducting electromagnet for particle accelerators but also for other applications of nuclear physics (energy spectroscopy, nuclear magnetic moments etc.), generator of a magnetic field of 2,5 T and uniformity $< 5\%$.
- Participation in the design, construction and testing of a cryogenic superconducting electromagnet cooling system at temperatures of 20 - 50 K), based on closed-cycle cooling systems, called cryocoolers;

- Implementation of state-of-the-art cryogenic cooling techniques (closed-cycle cryocoolers G-M type), with two cooling stages that require numerical modeling and thermal design of the cooling system that works by conduction and not by the classical use of cryogenic agents.

C.3. Development perspectives

Due to the advantages of HTS superconducting materials (much higher current carrying capacity, the generation of much larger magnetic fields than with conventional materials, significantly reduced mass and volume compared to conventional machines), in the field of electrical engineering, they will know an intense development in perspective.

For now, the small number of applications is due to the relatively high cost of producing these HTS superconducting materials, but the outlook is optimistic, in the sense of expecting the price to fall sharply.

The main interest in electrical engineering for HTS materials is the manufacture of superconducting coils, used in the production of electric machines and superconducting electromagnets for various applications whether research, industry, medicine or transportation.

The main reasons that make the use of HTS materials in electrical engineering and especially in the production of HTS superconducting electromagnets to be attractive, is the possibility of generating a stronger magnetic field (5 - 20 T) and the absence of Joule losses. The superconducting electromagnets (dipolar, quadripolar and sextupolar) in particle accelerators are made mainly of LTS superconducting materials (NbTi and Nb3Sn) and which are cooled with liquid helium (4,2 K). There is a major interest in replacing them with electromagnets made with HTS materials due to their much more economical operation, cryogenic cooling being able to be done with liquid nitrogen (77 K), which greatly reduces the costs. As a result, in the near future, our efforts will be part of this trend, which is also a technical and scientific challenge due to the problems that must be overcome and solved by introducing HTS materials in the construction of these electromagnets. Another development of interest is the obtaining of HTS electromagnets for the manufacture of MRI systems of medical imaging. The interests are of the same order: much more economical operation and superior performance. Thus, the introduction in the development of these types of HTS superconducting solenoids of the newest material, MgB2, is particularly promising due to the low price of obtaining it.

Another important direction of current and future development is to obtain intense magnetic fields where HTS materials (BSCCO and YBCO) have proven to be very suitable due to Hc_2 critical fields of much higher value than LTS (approximately 100 T).

Thus, HTS superconducting coils are and will be the basis of all future developments of electromagnets and generators of intense magnetic fields or high gradients of magnetic field and obviously of superconducting electric machines (motors and generators) with high operating efficiency. The transport of energy will be done through the use of superconducting cables, a reality already present in some countries. At the same time, medicine will benefit through the

development of high-performance MRI devices, but also transport through the development of high-speed trains, which have already become a reality.

BIBLIOGRAPHY

[1] *C.P. Poole Jr.*, *Handbook of Superconductivity*, ISBN: 0-12-561460-8, Library of Congress Catalog Card Number: 99-60091, Academic Press, 2000.

[2] http://cmms.triumf.ca/theses/Sonier/PhD/node7.html

[3] *C. Mantea, I. Puflea*, *Teorii Fenomenologice ale Supraconductibilității*, Editura Electra, 2006, ISBN (10) 973-7728-64-5, ISBN (13) 978-973-64-7.

[4] *S.S. Kalsi*, *Applications of High Temperature Superconductors to Electric Power Equipment*, Wiley-IEEE Press, ISBN: 978-0-470-16768-7, April 2011.

[5] *American Superconductor*, http://www.amsc.com/index.html, 2012.

[6] *Sumitomo Heavy Industries Ltd.*, http://www.shicryogenics.com/.

[7] *L.J. Masur, J.Kellers, F.Li, S.Fleshler, E.R. Podtburg*, "Industrial high temperature superconductors: perspectives and pilestones", IEEE Trans. Appl. Superconductivity, **12**, *1*, pp. 1145 – 1150, mai 2002.

[8] *J. Nagamatsu, N. Nakagawa, T. Murakana, Y. Zenitani, J. Akimitsu*, "Superconductivity at 39K in magnesium diboride", Nature, **410**,pp. 63-64, 2001.

[9] *Hyper Tech Research*, http://www.hypertechresearch.com/, 2010.

[10] *K. Berger, et. al.*, "Influence of temperature and/or field dependences of the E-J power law on trapped magnetic field in bulk YBaCuO", IEEE Trans. Appl. Supercond., **17**, *2*, pp. 3028 -3031, 2007.

[11] *E. Barzi, L.Del Frate, D. Turrioni, R. Johnson, M. Kuchnir*, "High temperature superconductors for high field superconducting magnets", Adv. Cryogenic Eng., **52**, p. 416, 2006.

[12] *R.M. Scanlan, A.P. Malozemoff, D.C. LarbaIes*, "Superconducting materials for large scale applications", Proc. IEEE, **92**, *10*, pp.1639-1654, 2004, DOI 10.1109 / JPROC.2004.833673.

[13] https://www.bruker.com/best.html.

[14] *L.J. Masur, J. Kellers, S. Kalsi, et al*., "Industrial HTS conductors: status and applications", EUCAS 2003, Sorento, Italy.

[15] http://www.qdusa.com/.

[16] *A.M. Morega, I. Dobrin, M. Popescu, M. Morega*, "Heat transfer analysis in the design phase of a high temperature superconductor motor", OPTIM 2010, 12th Conference, 22-24 May 2010, Brasov, Romania.

[17] *SuperPower*, https://www.superpower-inc.com/, 2012.

[18] *P.M. Grant*, "Potential electric power applications for magnesium diboride", The Industrial Physicist, **7**, *22*, 2001.

[19] *W.-J. Yeh, L. Chen, F. Xu, B. Bi, P. Yang,* "Persistent current in Ba-Y-Cu-O in liquid nitrogen", Phys. Rev., **B 36**, p. 2414, 1987.

[20] *Y. Shiohara, T. Taneda, M. Yoshizumi*, "Overview of materials and power applications of coated conductors project", Japanese Journal of Applied Physics, **51**, (2012), 010007.

[21] *N. Amemiya, N. Enomoto, S. Shirai*, "FEM analysis of AC loss in twisted Bi-2223 multifilamentary tapes carrying AC transport current in ac transverse magnetic field with arbitrary orientation", IEEE Trans. on Applied Superconductivity, **14**, *2*, June 2004.

[22] *F. Metani, J. Jiang, M. Matras, D.C. Larbalestier*, "Comparison of growth texture in round Bi2212 and flat Bi2223 wires and its relation to high critical current density development", Scientific Reports, **5**, pp. 8285, februarie 2015.

[23] *A.P. Malozemoff, S. Annavarapu, L. Fitzemeier, Q. Li, V. Prunier, M. Rupich. C. Thieme, W. Zhang, A. Goyal, M. Paranthaman, D.F. Lee*, "Low-cost YBCO coated conductor technology", Superconductor Science & Technology, **13**, *5*, p. 473, 2000.

[24] *D. Verebelyi, E. Harley, J. Scudiere, A. Otto, U. Schoop, C. Thieme, M. Rupich, A. Malozemof*, "Practical neutral axis conductor geometries for coated conductor composite wire", Supercond. Sci. Technolo., **16**, pp. 1158-1161, 2003.

[25] *D. Verebelyi, U. Schoop, C. Thieme, et al.*, "Uniform performance of continuously processed MOD-YBCO coated conductors using a textured Ni-W substrate", Supercond. Sci. Technol, **16**, pp. 19-23, 2003.

[26] *X. Xiong, K.P. Lenseth, J.L. Reeves, Y. Qiao, R.M. Schmidt, Y. Chen, Y. Li, Y-Y Xic, V. Selvamanicm*, "High throughput processing of long-length IBAD MgO and Epi-Buffer templates at SuperPower", Paper 4MA3, Presented at the IEEE Applied Superconductivity Conference, August 2006.

[27] *R. Flukiger, H.L. Suo, N. Musolino, C. Benedict, P. Toulemonde, P. Lezza*, "Superconducting properties of MgB_2. Tapes and wires", Physica, **385**, pp. 286-305, 2003.

[28] *C.I. Mocanu, Teoria Câmpului Electromagnetic*, Editura Didactică și Pedagogică, 1981

[29] *A.M. Morega, Principles of Heat Transfer*, Chapter VII in Mechanical Engineer's Handbook, Ed. D.B. Marghitu, Academic Press 2001, ISBN: 012471370X, pp. 446-557.

[30] https://www.shicryogenics.com/

[31] https://chemistry.illinois.edu/system/files/inline-files/Dean%20Giolando.pdf

[32] https://indico.cern.ch/event/286275/contributions/651700/attachments/531414/732823/JUAS_14_lect_1_intro__matls.pdf

[33] https://www.bnl.gov/magnets/hts-magnet-program.php

[34] https://www.imaios.com/en/e-Courses/e-MRI/MRI-instrumentation-and-MRI-safety/Magnets

[35] https://www.fnal.gov/

[36] *PANDA*, https://www.gsi.de/work/forschung/pandahsd.htm

[37] https://www.fujikura.co.uk/products/energy-and-environment/2g-ybco-high-tempurature-superconductors/

[38] https://www.nipne.ro/facilities/facilities/

[39] https://www.nuclearvacuum.eu/index.php

[40] http://www.jinr.ru/main-en/

[41] https://www.cem.tu-darmstadt.de/researching/topics/superconductivity/index.en.jsp

[42] http://www.icpe-ca.ro/icpe-ca/pdf/raport-nucleu-2009.pdf

[43] https://home.cern/

[44] *A.M. Morega, I. Dobrin, M. Morega, D. Enache*, "Înfășurare supraconductoare pentru câmp magnetic iniform, intens", Simpozionul de Mașini Electrice (SME 2015), Bucuresti, Romania.

[45] https://www.comsol.com/

[46] https://isis2.cc.oberlin.edu/physics/dstyer/Electrodynamics/MaxwellStressTensor.pdf

[47] *I. Dobrin, A.M. Morega, D. Enache, A. Dobrin, M. Morega, A. Dobre, I.R. Popovici*, "High temperature superconductor dipolar magnet for high magnetic field generation – design and fabrication elements", The 10th International Symposium on ADVANCED TOPICS IN ELECTRICAL ENGINEERING - ATEE 2017, Bucuresti.

[48] *O. Culha, I. Birlik, M. Toparli, E. Celik, S. Engel, B. Holzapfel*, "Characterization and determination of mechanical properties of YBCO superconducting thin films with

manganeseusing the tfa-mod method", ISSN 1580-2949.

[49] *J.W. Ekin, Experimental Techniques for Low-Temperature Measurements – Cryostat Design, Material Properties, and Superconductor Critical-Current Testing*, Oxford Univeristy Press, 2006, ISBN 0-19-857054-6; 978-0-19857054.

[50] *Y. Iwasa, Case Studies in Superconducting Magnets Design and Operational Issues Second Edition*, ISBN: 978-0-387-09799-2, e-ISBN: 978-0-387-09800-5, DOI: 10.1007/b112047, Library of Congress Control Number: 2009922081, © Springer Science+Business Media, LLC 2009.

[51] *D. Enache, I. Dobrin, A.M. Morega, M. Morega, A. Dobrin*, "Experiments on YBCO tape type high temperature superconductor junctions", (The International Conference on Applied and Theoretical Electricity ICATE 2016), Craiova, Romania, ISBN: 978-1-4673-8562-6.

[52] https://www.lakeshore.com/

[53] http://www.icpe-ca.ro

[54] https://www.epotek.com/

[55] https://www.edwardsvacuum.com/en

[56] https://www.hioki.com/en/products/detail/?product_key=5832

[57] https://www.tek.com/keithley

[58] http://www.americanmagnetics.com/index.php

[59] *A.M. Morega, I. Dobrin, M. Morega*, "Thermal and magnetic design of a dipolar superferric magnet for high uniformity magnetic field", 7th International Symposium on Advanced Topics in Electrical Engineering - ATEE, pp. 589-592, May 2011, ISBN 978-1-4577-0507-6.

[60] *I. Dobrin, A.M. Morega, D. Enache, A. Dobrin, I. Popovici, S. Zamfir*, "Bobine supraconductoare pentru acceleratoare de particule şi sistemul criogenic de răcire al acestora", Simpozionul de Maşini Electrice SME'16 ediţia a XIIa 11 Noiembrie 2016 FIE-UPB Bucureşti, pp. 2067-4147.

[61] *A. Bartalesi*, "Design of high field solenoids made of high temperature superconductors", pp. 2008-2009.

[62] *N.N. Balashov, P.N. Degtyarenko, S.S. Ivanov*, "Investigation of soldered low-resistance joints for coated conductors", Progress in Superconductivity and Cryogenics, **17**, *1*, pp. 25-27, 2015.

[63] *G. Celentano et al.*, "Electrical and mechanical characterization of coated conductors lap joints", IEEE Transactions on Applied Superconductivity, **20**, 2010.

[64] *D.K. Park et al.*, "Analysis of a joint method between superconducting YBCO coated conductors", IEEE Transactions on Applied Superconductivity, **17**, 2007.

[65] *M. Sugano et al.*, "Stress tolerance and fracture mechanisms of solder joint of YBCO coated conductors", IEEE Transactions on Applied Superconductivity, **17**, 2007.

[66] *I. Dobrin, A. Chernikov et al.*, "A 4T HTS magnetic field generator conduction cooled for condensed matter studies by neutron scattering", IEEE Transactions on Applied Superconductivity, January 2016.

[67] *T. Lecrevisse, J.M Ghellera, O. Loucharta, J.M Reya, P. Tixador*, "Critical current and junction between pancake studies for HTS coil design", Physics Procedia, **36**, *2012*, pp. 681-686, 2011.

[68] *D. Enache, I. Dobrin, A.M. Morega, S. Apostol*, "Superconductive dipolar electromagnets for particle accelerators. Two constructive models", Proc. of the 10th international Conference on electromechanical and power systems, pp. 351-355, 2015, ISBN 978-606-567-284-0.

[69] *A.M. Morega, I. Dobrin, M. Morega, A. Nedelcu, V. Stoica*, "Design and numerical simulations of a superconducting dipolar electromagnet cooled by conduction", The 9th International Symposium on Advanced Topics in Electrical Engineering ATEE 2015, pp. 79-83, May 7–9,

2015, ISBN 978-1-4799-7514-3.

[70] *A.M. Morega, I. Dobrin, M. Morega*, "Thermal and magnetic design of a dipolar superferric magnet for high uniformity magnetic field", Proc. 7th Int. Symp. (ATEE), pp. 589-592, May 2011.

[71] *Y. Dai et al*., "An 8T superconducting split magnet system with large crossing warm bore", IEEE Trans. Appl. Supercond., **20**, *3*, pp. 608-611, Jun. 2010.

[72] *E. Demikhov, F. Kostrov, V. Lysenko, N. Piskunov, V. Troitskiy*, "8T cryogen free magnet with variable temperature insert using a heat switch", IEEE Trans. Appl. Supercond., **20**, *3*, pp. 612-615, Jun. 2010.

[73] *F. Giebler, G. Thummes, K.J. Best*, "A 5 T persistent current niobium-titanium magnet with 4 K pulse tube cryocooler", Supercond. Sci. Technol., **17**, *5*, pp. 135-139, 2004.

[74] *J. Shi et al*., "Development of conduction cooled HTS SMES", IEEE Trans. Appl. Supercond., **17**, *3*, pp. 3846-3850, Sep. 2007.

[75] http://www.hts-110.com/currentleads.

[76] http://www.superox.ru/en/.

[77] *K.L. Kim et al*., "Feasibility study for elimination of the screening currents-induced fields in HTS coils", J. Supercond. Nov. Magn., **28**, pp. 83-88, 2015.

[78] *H. Miyazaki, S. Iwai, T. Tosaka, K. Tasaki, Y. Ishii*, "Degradation-free impregnated YBCO pancake coils by decreasing radial stress in the windings, method for evaluating delamination strength of YBCO-coated conductors", IEEE Trans. Appl. Supercond., **24**, *3*, pp. 1-5, Jun. 2014.

[79] *I. Dobrin, I. Puflea, N. Stancu, S. Zamfir*, "Magnet Superferic Dipolar pentru acceleratoare de particule", Rev. EEA, **58**, pp. 39-42, 2010.

[80] *I. Dobrin, Dipole Superferric Magnet*, 2010

[81] *M. Britcliffe, T. Hanson, J. Fernandez*, "A 2.5-Kelvin Gifford-McMahon/Joule-Thomson cooler for cavity maser applications", IPN Progress Report, pp. 42-147, Nov. 2001.

[82] http://www.dupontteijinfilms.com/.

[83] *A. Bejan, Heat Transfer*, NY:Wiley, 1998.

[84] *A.M. Morega, I. Dobrin, M. Morega*, "Thermal and magnetic design of a dipolar superferric magnet for high uniformity magnetic field", The 7th International Symposium on Advanced Topics in Electrical Engineering-ATEE, May 12-14, Bucharest, pp. 589-592, 2011, IEEE no: CFP1114P-PRT, ISBN 978-1-4577-0507-6.

[85] *I. Dobrin, A.M. Morega, A. Nedelcu, M. Morega, D. Daniel*, "Thermal and magnetic design of a HTS high magnetic field generator using superconducting Helmholtz coils", The 18th ICIT Conference with international participation Progress in Cryogenics and Isotopes Separation, October 2012.

[86] *A.M. Morega, I. Dobrin, A. Nedelcu, M. Morega*, "A quadrupolar superferric magnet", OPTIM 2012 13th International Conference on Optimization of Electrical and Electronic Equipment, pp. RD-006777, 24–26 May 2012.

[87] *K.L. Kim et al*., "Feasibility study for elimination of the screening currents-induced fields in HTS coils", J. Supercond. Nov. Magn., **28**, pp. 83-88, 2015.

[88] *I. Yukikazu, Case Studies in Superconducting Magnets*, Springer-Verlag, 2009.

[89] *N.V. Zamfir et al*., "Extreme Light Infrastructure: nuclear physics", Proc. SPIE, **8080**, 2011.

[90] *G. Suliman et al*., "Gamma-Beam industrial applications at ELI-NP", Romanian Reports in Physics, **68**, pp. 799-845, 2016.

[91] *S. Balascuta, I.C.E. Turcu*, "A conceptual design of an electron spectrometer for ELI-NP", AIP

Conf. Proc, pp. 296-300, 2015.

[92] *W. Kappel, N. Stancu et al*., "Magnetic automated installation for Yu Mo spectrometer", Revue Roumaine Des Sciences Techniques-Serie Electrotechnique et Energetique, **53**, *2*, pp. 79-84, 2008.

[93] *J. Tanabe, Iron Dominated Electromagnets*, World Scientific, 2005.

[94] *A.B. Holder, H. Keller*, "High-temperature superconductors: underlying physics and applications", Zeitschrift für Naturforschung B, **75**, *1-2*, DOI: https://doi.org/10.1515/znb-2019-0103, 2019.

[95] *A. Devred, Practical Low-Temperature Superconductors*, https://cds.cern.ch/record/796105/files/CERN-2004-006.pdf.pdf, CERN, 2004

[96] *R. Zeng, V. Murashov, T.P. Beales, H.K. Liu, S.X. Dou*, "High temperature superconducting magnetic levitation train", Applied Superconductivity, **5**, *1–6*, January–June 1997, pp. 201-204.

[97] *W.V. Hassenzohl, D.W. Hazelton, B.K. Johnson, Ch.T. Reis*, "Electric Power Applications", Proceedings of the IEEE, **92**, *10*, Oct. 2004.

[98] *Santosh Miryala, Recent Superconducting Applications in the Medical Field*, High Temperature Superconductors, ISBN 978-1-53613-341-7, Nova Science Publishers, Inc., 2018., Chapter 15.

[99] https://www.luvata.com/products/ultra-pure-copper-products

[100] *D.Bruce Montgomery, Solenoid Magnet Design. The Magnetic and Mechanical Aspects of Resistive and Superconducting Systems*, Interscience (Wiley), New York, 1969.

[101] https://kgw-isotherm.com/

[102] https://trc.nist.gov/cryogenics/materials/OFHC%20Copper/OFHC_Copper_rev1.htm

[103] http://www.sunpowerinc.com/

[104] *J. Minervini, M. Parizh, M. Schippers*, "Design of a HTS cuadrupolar magnet focus on superconducting magnets for hadron radiotherapy and MRI", Superconductor Science and Technology, **31**, *3*, 2018

[105] *E. Darie, E. Darie*, "Fault current limiters based on high temperature superconductors", 8th International Conference on Electric Fuses and their Applications, Clermont-Ferrand, 2007, pp. 69-73, doi: 10.1109/ICEFA.2007.4419969.

[106] *I. Dobrin, D. Enache, A. Dobrin, G. Dumitru*, "Numerical modeling and design of a superconducting solenoid generator of 6T magnetic flux density", Scientific Bulletin of University Politehnica of Bucharest, 2020.